Desalination and Water Treatment
www.deswater.com

doi: 10.5004/dwt.2023.29489

292 (2023) 152–164
April

Efficient removal of humic acid from aqueous solutions using three-dimensional/magnetic graphene oxide allylamine/allyl glycidyl ether: optimization by Taguchi design method

Sanaz Jafari[a], Amir Hossein Javid[a,*], Elham Moniri[b], Amir Hessam Hassani[a], Homayon Ahmad Panahi[c]

[a]*Department of Environmental Engineering, Science and Research Branch, Islamic Azad University, Tehran, Iran, Tel.: +989121037369; emails: a.javid@srbiau.ac.ir (Amir H. Javid) ORCID: 0000-0003-1766-8827, sani_sjafari@yahoo.com (S. Jafari), hhassani@srbiau.ac.ir (Amir H. Hassani)*
[b]*Department of Chemistry, Varamin (Pishva) Branch, Islamic Azad University, Varamin, Iran, email: moniri30003000@yahoo.com*
[c]*Department of Chemistry, Central Tehran Branch, Islamic Azad University, Tehran, Iran, email: h.ahmadpanahi@iauctb.ac.ir*

Received 7 September 2022; Accepted 7 March 2023

ABSTRACT

We developed a novel three-dimensional graphene oxide/allylamine/allyl glycidyl ether, and evaluated its adsorption performance for humic acid removal in an aqueous solution. The effective parameters were optimized by the Taguchi design method. Effective parameters on the removal of humic acid, including adsorbent dosage, solution pH, contact time, and temperature were evaluated using an L_9 orthogonal array. The optimum parameters were adsorbent dosage of 0.02 g, pH of 6, contact time of 120 min, temperature of 25°C, and the removal efficiency of humic acid was 58%. Also, analysis of variance showed the most significant factors were adsorbent dosage and contact time with 33.58% and 51.62% contribution, respectively. The prepared nanoadsorbent was characterized by Fourier-transform infrared spectroscopy, field-emission scanning electron microscopy with energy-dispersive X-ray analysis, and thermogravimetric analysis. The equilibrium data were evaluated by different isotherm models, where the data followed a Langmuir model with a maximum sorption capacity of 25.97 mg/g. Also, the kinetic adsorption data were well evaluated by the pseudo-second-order model. The thermodynamic data shown that the sorption of humic acid onto the nanoadsorbent was an exothermic, favorable, and spontaneous process. The regeneration test indicated that the nanoadsorbent could be reused in the water treatment application. This study concluded that nanoadsorbent is a very hopeful nanoadsorbent for the remediation of water polluted by humic acid.

Keywords: Humic acid; Taguchi design; Three-dimensional; Magnetic graphene oxide; Allyl glycidyl ether

1. Introduction

Humic acid (HA), the major of natural organic matter, was ubiquitously present in the natural environments, such as surface water, drinking water, and groundwater as a result of the biological decomposition from animals, plants, and other microorganisms in natural systems. Plenty of carboxyl, phenolic hydroxyl, and carbonyl groups in HA structures result in high chemical reactivity and structural complexity. HA may cause environmental water to have an undesirable taste and bind heavy metals and other organic matter to increase their concentrations in water. HA may react with chlorine disinfectants to form carcinogenic disinfection by-product during the chlorination step in water

* Corresponding author.

production. Accordingly, the removal of HA from water samples is of significant importance [1–3].

The elimination of water samples containing HA has been considered by several methods such as adsorption [4], coagulation [5], photo-catalytic oxidation [6], membrane filtration [7], and advanced oxidation [8]. One of the most essential methods for the removal of low concentrations of organic pollutants is adsorption [9–11].

Due to the existence of functional groups such as carboxyl, hydroxyl, and epoxy groups along with a delocalized π-electron system, graphene oxide (GO) is an ideal adsorbent of positively charged nanomaterials [12]. Due to their low price, low toxicity, functional controllability, and quickly separation in the magnetic field, magnetic nanoparticles have attracted wide attention [13]. One of the most essential magnetic adsorbents is related to iron oxides, which are easy eroded and oxidized in an aqueous solution [14]. Silica has been used as an ideal coating layer to protect the magnetic core, such as Fe_3O_4/SiO_2 core/shell nanoparticles attached to graphene oxide [15], magnetic ethylenediaminetetraacetic acid-modified chitosan/SiO/Fe_3O_4 [16], amino-functionalized Fe_3O_4@SiO_2 [17], and thiol modified Fe_3O_4@SiO_2 [18], due to the ease of subsequent functionalization of SiO_2 and chemical stability.

In recent years, many research based on magnetic GO have been reported. For example, Yang et al. [19] prepared a thiourea-dioxide–reduced magnetic graphene oxide for the removal of HA. In addition, Wang et al. [20] groups developed the polyethylenimine-modified magnetic mesoporous silica and graphene oxide (MMSP-GO) [20].

Moreover, there have been many studies used three-dimensional (3D) graphene composites or their derivatives in practical applications, which has resulted in an appropriate sorption capacity for different contaminants [21]. Nowadays, there is little study about 3D/GO to remove HA from water samples, and HA removal needs to be further enhanced. Herein, a 3D/GO was developed through modification of GO by allylamine/allyl glycidyl ether (AA-AGE), followed by freeze drying as a reusable and non-toxic nanoadsorbent for HA removal from the aqueous solution. Taguchi design as a statistical experiment optimization was performed to study influences of four factors on the HA adsorption. The magnetic nanoadsorbent was characterized by analytical techniques. The adsorption and desorption mechanisms of HA in solution on the nanoadsorbent were investigated. The associated sorption mechanism was also studied.

2. Experimental section

2.1. Materials

The HA used in this work was purchased from Sigma-Aldrich (Steinheim, Germany). A stock solution of HA (1,000 mg/L) was prepared by dissolving 1 g of HA powder in 1 L of distilled water. A few drops of NaOH solution (1 N) were also added to complete the dissolving of HA. All chemicals such as multilayer GO, AA (C_3H_7N), AGE ($C_6H_{10}O_2$), azobisisobutyronitrile ($C_8H_{12}N_4$; AIBN), 1,3,5-trihydroxybenzene ($C_6H_6O_3$; PG), iron(III) chloride hexahydrate ($FeCl_3{\cdot}6H_2O$), iron(II) chloride tetrahydrate ($FeCl_2{\cdot}4H_2O$), dimethyl sulfoxide (DMSO), sulfuric acid (H_2SO_4), nitric acid (HNO_3), and ethanol (C_2H_5OH; EtOH) were purchased from Merck, Darmstadt, Germany. A Millipore water purification system (Milli-Q, Bedford, USA, ≥18 MΩ) was used to obtain ultrapure water.

2.2. Characterization

The morphology and the elemental analysis of the products were detected by using a field-emission scanning electron microscopy (FE-SEM: TESCAN MIRA 3-XMU Brno, Czech Republic) and energy-dispersive X-ray spectrometer (EDX), respectively. Thermogravimetric analysis (TGA) was conducted using STA449F3 TGA (Netzsch, Germany) at the rate of 10°C/min in a nitrogen atmosphere at 20°C–600°C). The Fourier-transform infrared spectra were recorded using an Fourier-transform infrared (FT-IR) spectrometer (AVATAR 360 ESP, USA) in the wave number range 4,000–400 cm^{-1}. The specific surface area of the nanoadsorbent was measured using Brunauer–Emmett–Teller (BET) method (Micromeritics ASAP 2020 model). The drying method of nanoadsorbent was carried out using a freeze dryer (Binder, Germany). The absorbance spectra were determined using a UV-Vis spectrophotometer (UV-2100, Japan) in the wavelength range of 200–800 nm. For the chromatographic tests, a high-performance liquid chromatography (HPLC) equipped with a UV detector was used. Chromatographic separations were carried out on a Bio Suite column (7.8 mm × 300 mm). A mixture of sodium phosphate, sodium sulfate, and sodium azide was used as the mobile phase at a flow rate of 1 mL/min. The injection volume and wavelength were 20 μL and 480 nm, respectively.

2.3. Preparation of the 3D/GO@AA-AGE/PG

2.3.1. Preparation of GO@AA-AGE/PG

The amount of GO (2 mg), 3 mL of H_2SO_4, and 2 mL of HNO_3 were stirred in a glass beaker for 20 min and subsequently centrifuged for 15 min at 3,000 rpm. Then, the product was washed to remove the organic compounds, and dried in a vacuum oven for 24 h. Next, the precipitate was titrated with a solution of AA (10 mL). The mixture was stirred for 3 h. After that, the above sediment was dispersed in 40 mL of EtOH and 10 mL of AGE, and the mixture was then perched for 5 min under N_2. After adding of AIBN (0.1 g), the mixture was stirred for 7 h at 65°C. The prepared sample was washed several times with deionized water and EtOH, and then dried. Finally, the amount of previously precipitate, 0.3 g of PG, 10 mL of acetate buffer, and 20 mL of DMSO solution were combined. Then, the resulting mixture was shaken at 40°C for 24 h. The prepared GO@AA-AGE/PG was washed and dried for subsequent experiments. Fig. 1 indicates the proposed schematic diagram of GO@AA-AGE/PG and mechanism of interaction between HA with GO@AA-AGE/PG.

2.3.2. Preparation of magnetic nanoparticles

The magnetic nanoparticles (MNPs) were synthesized based on the co-precipitation method [22]. Based on this method, 5.4 g of $FeCl_3{\cdot}6H_2O$ and 2 g of $FeCl_2{\cdot}4H_2O$ were dispersed in deionized water (200 mL) in a three-neck flask and stirred for 30 min. Afterward, the mixture was stirred

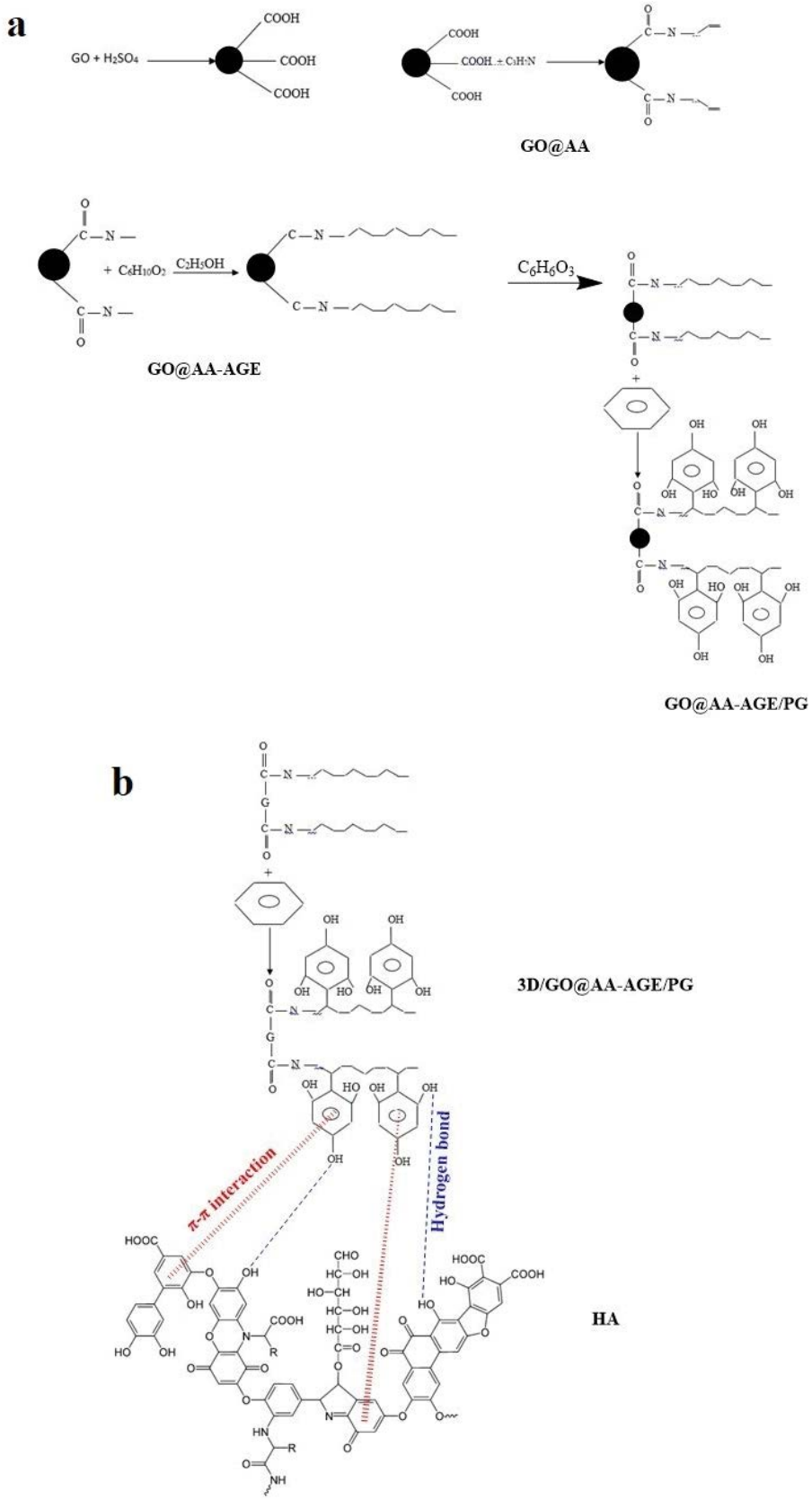

Fig. 1. (a) Schematic mechanism of GO@AA-AGE/PG and (b) possible mechanism of interaction between humic acid with GO@AA-AGE/PG.

at 80°C under N_2 gas. Subsequently, 40 mL of ammonium hydroxide was added drop by drop to the above solution for 2 h until the color of the solution changed to black. After ultrasonication, the mixture was collected via the external magnet, washed, and dried at 70°C for 12 h.

2.3.3. Preparation of 3D/GO@AA-AGE/PG

Firstly, 0.2 g of GO@AA-AGE/PG was added to 100 mL of deionized water, and the pH of the solution was adjusted to 11 by adding ammonium hydroxide solution. Next, 0.965 g of MNPs was added to the above mixture. The solution was stirred at a temperature of 90°C for 6 h. Finally, the products were washed three times with water and dried at –70°C for 24 h in a freeze dryer.

2.4. Taguchi design

To reduce the number of tests and to identify the main influences of factors, we used Taguchi orthogonal array design (L_9). For this purpose, four independent factors were evaluated at three levels, high (+3), center (+2), and low (+1). The factors included pH (3, 6, 9), adsorbent dosage (0.002, 0.02 and 0.035 g), contact time (5, 35 and 120 min), and temperature (25°C, 38°C, and 50°C). All tests were repeated three times. Table 1 shows all of the factors and levels used in this test. Also, A L_9 orthogonal array as shown in Table 2.

2.5. Batch adsorption tests

The sorption of HA onto 3D/GO@AA-AGE/PG was investigated in batch tests. To obtain the optimum conditions for adsorbent dosage (0.002–0.035 g), temperature (25°C–50°C), contact time (5–180 min), and pH (3–9) were assessed by Taguchi orthogonal array design. The adsorption tests were performed in a flask containing 25 mL of HA solution with 25 mg/L. The solution, which was adjusted to pH 6 and contained 0.02 g of 3D/GO@AA-AGE/PG, was added and shaken for 120 min at 25°C. Next, the solution was centrifuged at 5,000 rpm for 10 min, and the residual concentration of HA was tested with the aid of a UV-Vis spectrophotometer (λ_{max} = 254 nm). The removal and adsorption capacity of HA were assessed with the following equations:

$$R\% = \frac{C_0 - C_e}{C_0} \times 100\% \quad (1)$$

$$q_e = \frac{\left(C_0 - C_e\right)V}{W} \quad (2)$$

where C_0 and C_e (mg/L) are the initial and equilibrium concentrations of HA, respectively. V (L) is the volume of the solution, and W (g) is the weight of the nanoadsorbent.

Table 1
Controllable parameters and their levels in the Taguchi method

Parameters	Level 1	Level 2	Level 3
pH	3	6	9
Adsorbent dosage, g	0.002	0.02	0.035
Contact time, min	5	35	120
Temperature, °C	25	38	50

Table 2
L_9 orthogonal array

Parameters				Run
Adsorbent dosage	Contact time	Temperature	pH	
1	1	1	1	1
1	2	2	2	2
1	3	3	3	3
2	1	2	3	4
2	2	3	1	5
2	3	1	2	6
3	1	3	2	7
3	2	1	3	8
3	3	2	1	9

2.6. Adsorption isotherms and kinetics

To investigate a sorption technique for HA sorption, it is necessary to obtain the most suitable correlation for equilibrium curves. In this regard, the sorption isotherm of HA onto 3D/GO@AA-AGE/PG was studied using the Langmuir, Freundlich, Temkin, Dubinin–Radushkevich isotherm models. To study the isotherm models, 0.015 g of 3D/GO@AA-AGE/PG was added to a series of micro-test tubes filled with the solutions of HA (2–100 mg/L). The micro-test tubes were shaken for 1 h. For the kinetic test, the micro-test tubes (20 mg/L) were vortexed for (5–150 min) at pH = 6. Three sorption kinetic models of pseudo-first-order, pseudo-second-order, and intraparticle diffusion models were used to investigate the experimental data.

2.7. Real samples

To investigate the applicability of the proposed technique for adsorption of HA, two kind of well water samples were collected and analyzed. The well water samples were taken from Darakeh (Tehran, Iran) and Manjilabad (Karaj, Iran). All samples were kept in dark glass bottles and filtered through a membrane filter (0.45 μm) before use. For the determination of HA in water samples, the samples were prepared at a concentration of 0.05 mg/L and 3D/GO@AA-AGE/PG was added to the solution, and stirred for 90 min at 25°C. Then, the solution was centrifuged. The adsorbed HA was eluted using 1 mL solution of mobile phase, stirred for 5 min, and 1 mL of the supernatant was taken out for analysis by the HPLC system.

3. Results and discussion

3.1. Nanoadsorbent characterization

3.1.1. Field-emission scanning electron microscopy/energy-dispersive X-ray spectroscopy

The particle size and surface morphology of 3D/GO@AA-AGE/PG were studied using FE-SEM images. As

observed in Fig. 2, the 3D/GO@AA-AGE/PG has a spherical shape with a uniform and smooth surface morphology with an average size of about 29 nm. To identify elemental compositions, the EDX analyses were carried out for 3D/GO@AA-AGE/PG. The successful formation of the 3D/GO@AA-AGE/PG was shown by the EDX spectrum, which presented the only presence of C, Fe, O, and N with weight percentages of 50.89, 1.76, 36.32, and 11.03 wt.%, respectively. The existence of N and Fe peaks along with C and O are evidence for the presence of Fe_3O_4 nanoparticles and AA polymer on the surface of 3D/GO@AA-AGE/PG.

3.1.2. Fourier-transform infrared spectroscopy

The successful preparation of 3D/GO@AA-AGE/PG was considered by using the FT-IR analysis, and the obtained spectra are indicated in Fig. 3. As can be seen in Fig. 3a, the peaks at 1,021; 1,559; 1,652; 2,985 and 3,428 cm^{-1} were related to the stretching vibration of C–O–C, C–N, C=C, C–H, and O–H groups on the GO surface. After the reaction with Fe_3O_4, the 3D/GO@AA-AGE/PG (Fig. 3b) indicated the peaks assigned for Fe–O at 596 cm^{-1}. The lower intensity of the 3D/GO@AA-AGE/PG bands compared to the GO could be a sign of the growth of the Fe_3O_4 nanoparticles from the GO@AA-AGE/PG surface.

3.1.3. Thermogravimetric analysis

TGA curves of GO@AA-AGE/PG and 3D/GO@AA-AGE/PG are shown in Fig. 4. For GO@AA-AGE/PG, the TGA curve shows three steps of thermal decomposition processes. As can be seen in Fig. 4a, the initial stage of weight loss there is around 120°C, the second stage is observed about 220°C, and the third stage is observed at about 400°C–600°C which is respectively associated with the removal of the water molecules, grafting of the organic compounds, and the degradation of GO backbone. For 3D/GO@AA-AGE/PG (Fig. 4b), a weight loss up to 50°C was associated to the desorption of water from the surface, the mass loss at 100°C–250°C was due to the degradation of organic compounds, and the weight loss at 300°C–600°C was related to the decomposition of the GO structure. Due to the exciting of Fe_3O_4 nanoparticles in the structure, the weight loss of 3D/GO@AA-AGE/PG is lower than that of GO@AA-AGE/PG.

3.1.4. Brunauer–Emmett–Teller-Barrett–Joyner–Halenda

Fig. 5a shows the N_2 adsorption–desorption isotherm measured by the BET method at 77 K. According to the International Union of Pure and Applied Chemistry, N_2 adsorption–desorption isotherm for 3D/GO@AA-AGE/PG belongs to typical type IV with H_3 hysteresis. The surface

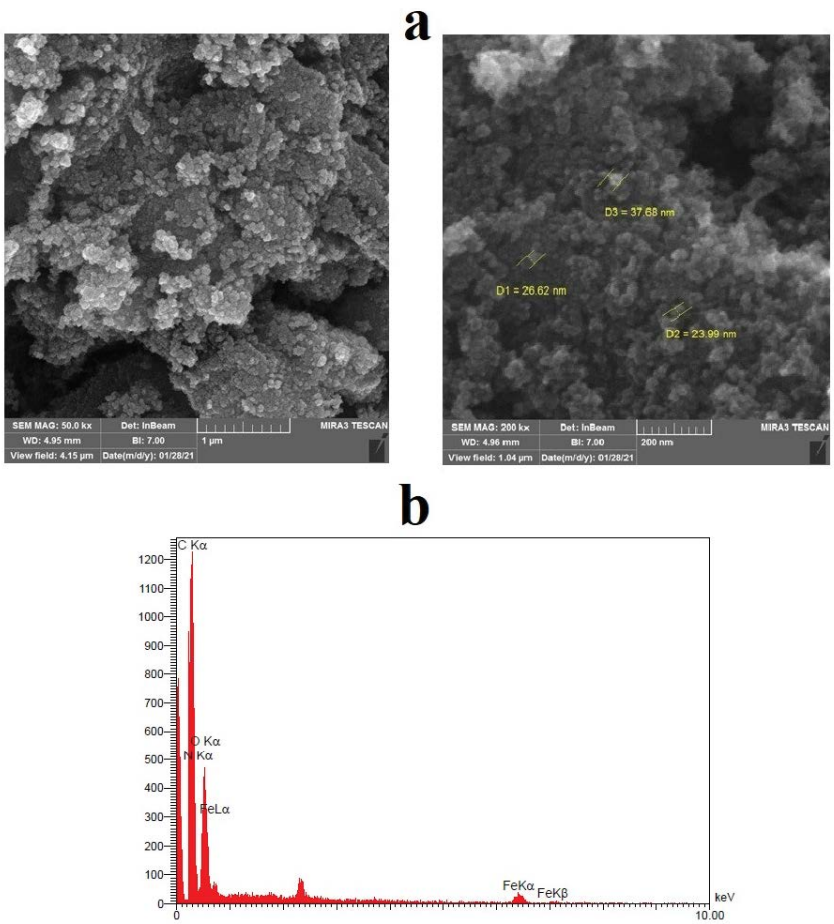

Fig. 2. (a) Field-emission scanning electron microscopy images and (b) energy-dispersive X-ray spectrum of 3D/GO@AA-AGE/PG.

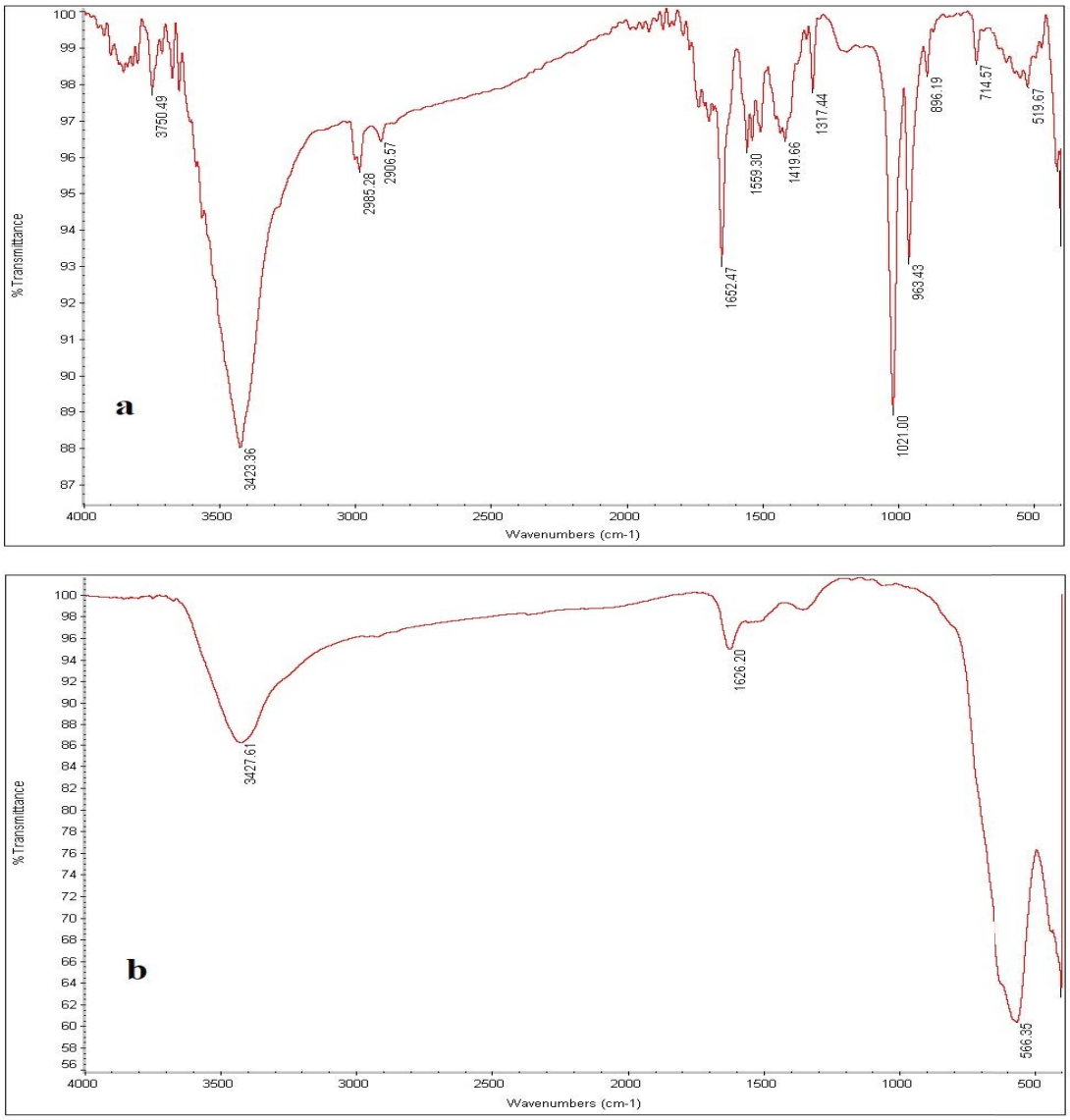

Fig. 3. Fourier-transform infrared spectra of the (a) GO and (b) 3D/GO@AA-AGE/PG.

area, pore size, and pore volume of 3D/GO@AA-AGE/PG were found to be 97.35 m^2/g, 10.30 nm, and 0.25 cm^3/g, respectively. In addition, Fig. 5b shows the BET plot of 3D/GO@AA-AGE/PG.

3.2. Optimization studies

The pH affects the states of the 3D/GO@AA-AGE/PG and HA. In this work, the pH was adjusted using magic buffer (1.43 mL of CH_3COOH (0.05 M), 1.67 mL of H_3PO_4 (0.06 M), 1.2 g of H_3BO_3 (0.04 M), and NaOH (2 M)) from 3 to 9. Fig. 6a shows the best data were detected at pH = 6. Low pH was not suitable because the HA was protonated. Also, when pH of the solution increased, the adsorption capacity of HA increased while the adsorption capacity of HA decreased significantly at higher values, maybe because HA was deprotonated at pH > 6, and a decrease in the sorption capacity. Consequently, pH = 6 was chosen for subsequent experiments.

The point of zero charge (PZC) was measured by using a plot that shows the final pH (pH_f) vs. initial pH (pH_i). These data are indicated in Fig. 6b. The PZC of the 3D/GO@AA-AGE/PG has positive and negative charge below and above pH_{pzc}, respectively. The PZC for 3D/GO@AA-AGE/PG is $pH_{pzc} = 6.5$.

The weight of 3D/GO@AA-AGE/PG commonly has significant effect on the adsorption capacity. In this study, different amounts of 3D/GO@AA-AGE/PG (0.002–0.035 g) were estimated (Fig. 6c). The adsorption capacity of HA increased when the adsorbent dosage increased from 0.002 to 0.02 g, and then decrease slowly with further increase of the adsorbent dosage from 0.02 to 0.035 g. So, 0.02 g of 3D/GO@AA-AGE/PG was used as the optimal amount.

For investigating the effect of the contact time on HA removal efficiency, contact times were changed in the range of 5–120 min. (Fig. 6d), presents the peak area ratio for HA which was increased with the contact time up to 90 min, and remained constant after that. Hence, 90 min of contact time

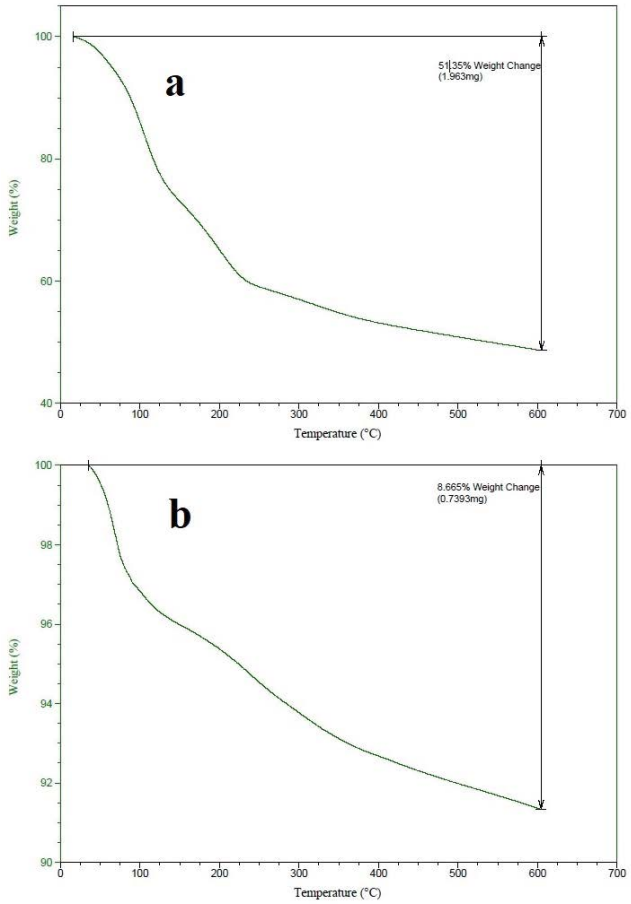

Fig. 4. Thermogravimetric analysis curves of the (a) GO@AA-AGE/PG and (b) 3D/GO@AA-AGE/PG.

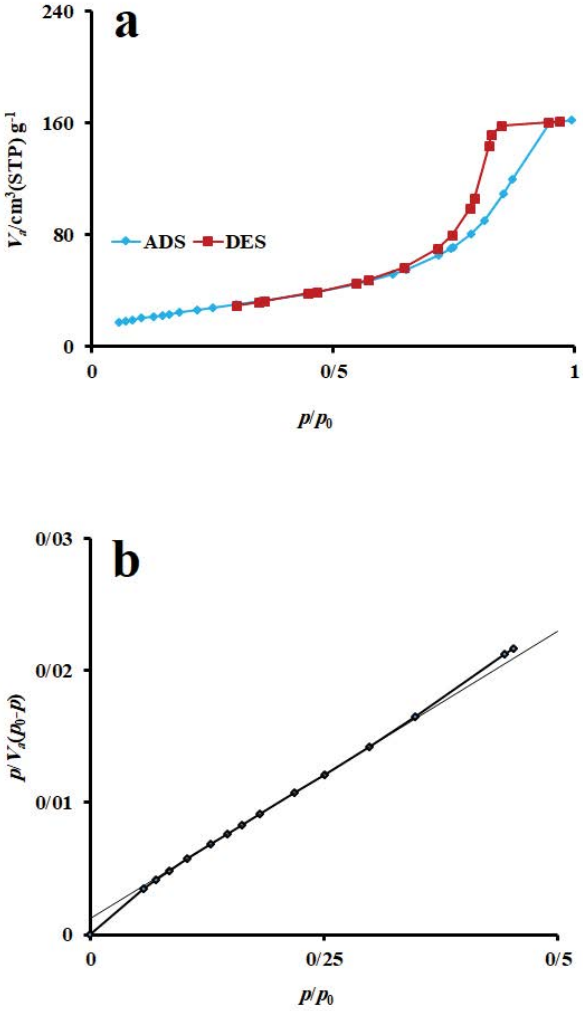

Fig. 5. (a) N_2 adsorption–desorption isotherm and (b) Brunauer–Emmett–Teller plot of 3D/GO@AA-AGE/PG.

was selected as the optimum time for subsequent experiments. Also, the half-time of saturation adsorption is about 20 min.

The effect of temperature from 25°C to 50°C on the removal efficiency of HA is indicated in (Fig. 6e). As can be seen, the removal efficiency of HA and its temperature decreased from 89% to 33% from 25°C to 50°C, respectively. Also, the influence of temperature on the adsorption capacity was smaller (11.9 to 4.5 mg/g) in the T > 25°C. The high temperature had a negative effect on the removal due to enhanced mobility of the HA in the aqueous solution.

3.3. Taguchi's method

Main effects plots indicate how each parameter especially affects the response. The main effects of adsorption efficiency for each factor at each level are plotted in Fig. 7. As shown in Fig. 7, the signal-to-noise (S/N) ratio graph indicates that the optimal parameter level necessary to achieve the best adsorption efficiency is A_2, B_1, C_3 and D_2 where A_2 = 0.02 g of adsorbent dosage, B_1 = temperature (25°C), C_3 = 120 min of contact time, and D_2 = pH of 6. Table 3 shows the analysis of variance (ANOVA) results of the model obtained from experimental data. According to Table 3, DOF = degree of freedom, MS = mean of square, SS = sum of square, and P% = contributing factor. As can be seen in Table 3, it is obviously observed that both adsorbent dosage and contact time have significant effect on the adsorption efficiency. Also, the highest values of SS (50.97) and MS (25.48) for the influencing factor 'A' (adsorbent dosage) and the highest values of SS (78.35) and MS (39.17) for the influencing factor '*C*' (contact time) are observed. Also, the P% is more for contact time which is 51.62%, while the adsorbent dosage has a P% of 33.58%. The P% of other factors, such as pH and temperature is negligible. Fig. 7 shows the actual P% of each parameter in adsorption efficiency. Also, the optimum performance and significant interaction for each factor are shown in Fig. 8.

3.4. Isotherms, kinetics, and thermodynamics studies

To investigate the sorption isotherm of 3D/GO@AA-AGE/PG, several mathematical models have been described. Here, Langmuir [23], Freundlich [24], Temkin [25], and Dubinin–Radushkevich [26] are the generally used models to evaluate the adsorption mechanism of 3D/GO@AA-AGE/PG, which is expressed by the following equation:

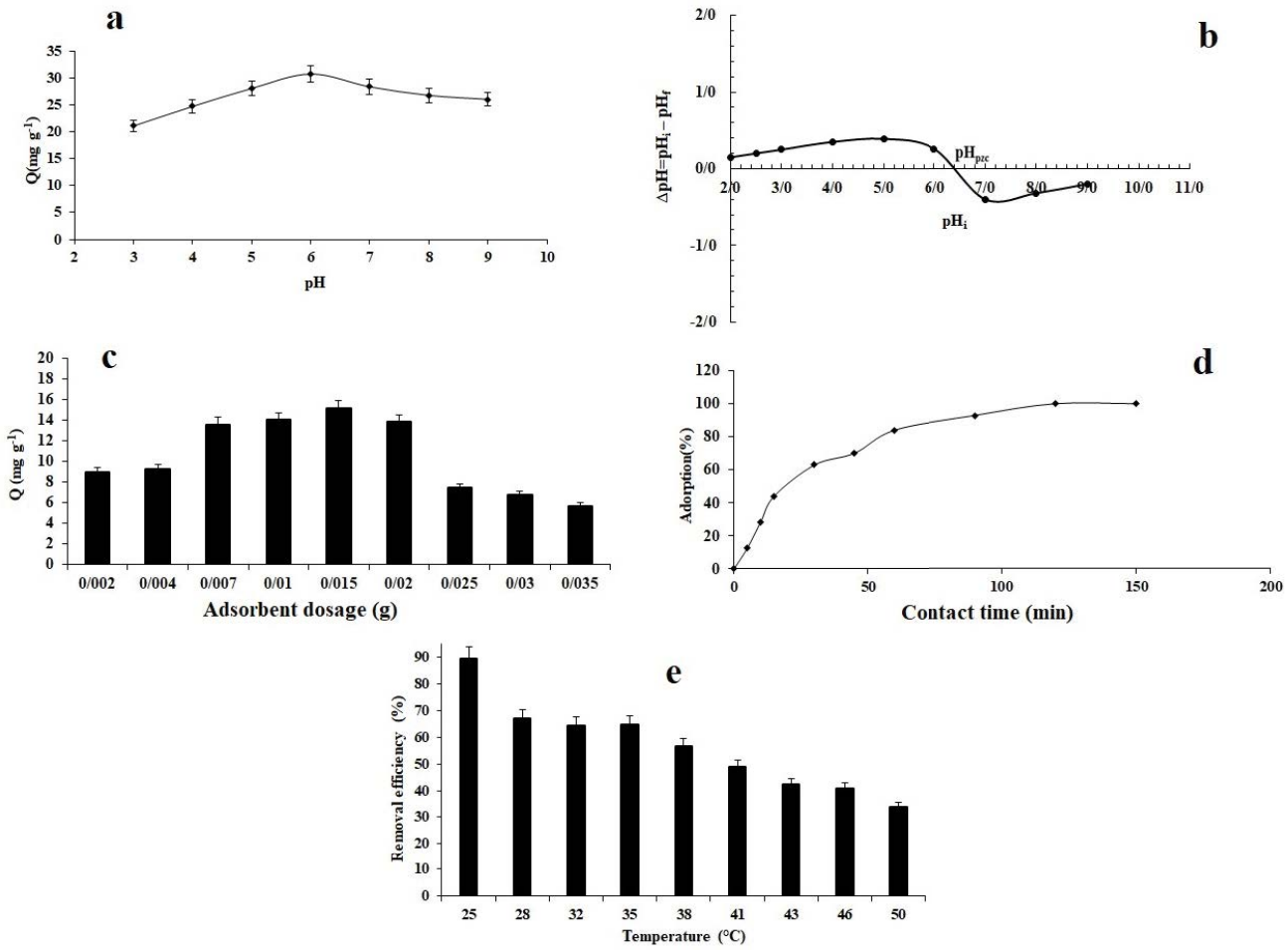

Fig. 6. Effect of (a) solution pH, (b) pH_{pzc}, (c) amount of adsorbent, (d) contact time, and (e) temperature on humic acid adsorption to 3D/GO@AA-AGE/PG.

Langmuir isotherm: $$\frac{C_e}{q_e} = \frac{1}{K_L q_{\max}} + \frac{C_e}{q_{\max}} \quad (3)$$

Freundlich isotherm: $$\ln q_e = \frac{1}{n}\ln C_e + \ln K_F \quad (4)$$

Temkin isotherm: $$q_e = B\ln C_e + B\ln K_T \quad (5)$$

Dubinin–Radushkevich isotherm: $$q_e = q_{\max}\exp\left(-\beta\varepsilon^2\right) \quad (6)$$

where $q_{\max}$ is the maximum sorption capacity of HA (mg/g), C_e is the concentration of HA at equilibrium (mg/L), q_e is the equilibrium adsorption capacity of HA (mg/g). Moreover, K_L (L/mg), K_F (mg/g)(L/mg)$^{1/n}$, and β (mol^2/kJ^2) are the Langmuir, Freundlich, and Dubinin–Radushkevich isotherm constant, respectively. Also, $B = RT/b$ and R (8.314 J/mol·K) is the universal gas constant, T (K) is the temperature, and b (J/mol) is the constant related to the heat of HA sorption. K_T (L/g) and ε [=RTln(1 + 1/C_e)] (kJ/mol) are the Temkin constant and the Polanyi potential, respectively. The calculated parameters of the isotherm models were listed in Table 4. The equilibrium data was fitted to the Langmuir isotherm model (R^2 = 0.9969) and the maximum adsorption capacity of 3D/GO@AA-AGE/PG was found to be 25.97 mg/L. According to the Freundlich isotherm model, the sorption mechanism will be desirable (1/n = 0–1).

To investigate the equilibrium time of the sorption mechanism, pseudo-first-order [27], pseudo-second-order [28], and intraparticle diffusion [29] kinetic models were evaluated. The equation of the kinetic models is expressed by the following equation:

Pseudo-first-order kinetic: $$\log\left(q_e - q_t\right) = \log q_e - \frac{K_1 t}{2.303} \quad (7)$$

Pseudo-second-order kinetic: $$\frac{t}{q_t} = \frac{1}{K_2 q_e^2} + \frac{t}{q_e} \quad (8)$$

Intraparticle diffusion kinetic: $$q_t = K_i t^{1/2} + C_i \quad (9)$$

where q_t and C_i are the sorption capacity at time (mg/g) and intercept, respectively. K_1 (min^{-1}), K_2 (g/mg·min), and K_i

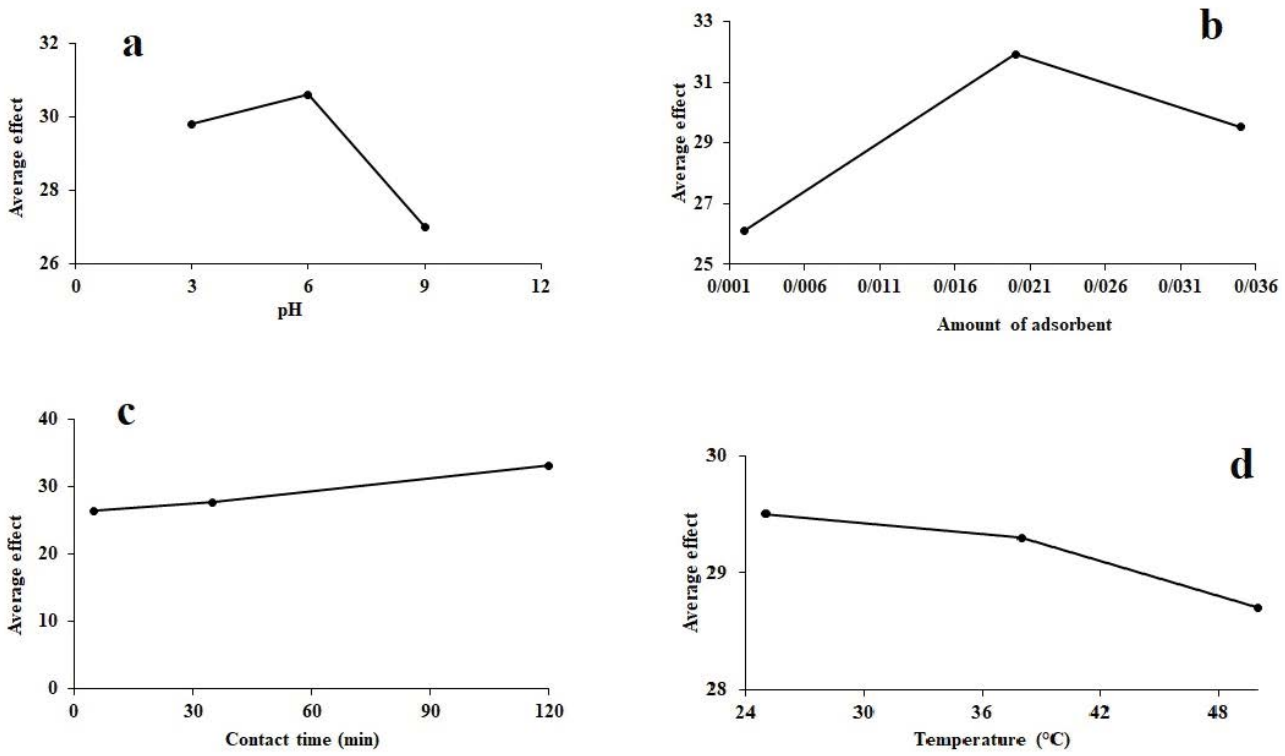

Fig. 7. Main effect of each factor by S/N ratios for different parameters: (a) pH, (b) amount of adsorbent, (c) contact time, and (d) temperature.

Table 3
Results of analysis of variance

Parameters	DF	SS	MS	P%
pH	2	21.350	10.675	14.066
Adsorbent dosage	2	50.978	25.489	33.587
Contact time	2	78.352	39.176	51.622
Temperature	2	1.097	0.548	0.723

Table 4
Calculated parameters of Langmuir, Freundlich, Temkin, and Dubinin–Radushkevich models

Model	Parameter	Value
Langmuir	q_{max} (mg/g)	25.97
	K_L (L/mg)	0.07
	R_L	0.13
	R^2	0.9969
Freundlich	n	1.70
	K_F (mg/g)(L/mg)$^{1/n}$	2.16
	R^2	0.9598
Temkin	K_T (L/g)	1.20
	B	525.65
	R^2	0.9768
Dubinin–Radushkevich	β (mol^2/kJ^2)	1×10^{-7}
	q_{max} (mg/g)	11.25
	R^2	0.9127

(mg/g·min$^{1/2}$) are the pseudo-first-order, pseudo-second-order and intraparticle diffusion rate constant, respectively. As shown in Table 5, the sorption mechanism follows the pseudo-second-order kinetic model. Also, the effects of the three kinetic models for the adsorption of the HA onto 3D/GO@AA-AGE/PG are indicated in Fig. S1.

To evaluate the sorption mechanism of the HA onto 3D/GO@AA-AGE/PG, thermodynamic parameters of enthalpy change (ΔH°, J/mol), free energy change (ΔG°, J/mol), and entropy change (ΔS°, J/mol·K) were applied to express the thermodynamic behavior of the sorption of the HA onto the adsorbent. The parameters were computed by the following equations:

$$\Delta G^\circ = -RT \ln K_L \tag{10}$$

$$\ln K_L = \frac{\Delta S^\circ}{R} - \frac{\Delta H^\circ}{RT} \tag{11}$$

where K_L is the thermodynamic equilibrium constant. The ΔS° and ΔH° can be calculated by plotting the lnK_L and 1/T as Fig. S2. The thermodynamics parameters of the HA onto nanoadsorbent were indicated in Table 6. The negative ΔG° values show spontaneous HA sorption to 3D/GO@AA-AGE/PG at all three temperatures. The positive ΔS° value suggests an increase in the randomness of the liquid/solid interface, with structural changes in the HA/3D/GO@AA-AGE/PG system. The negative ΔH° value confirms the exothermic nature of the sorption procedures.

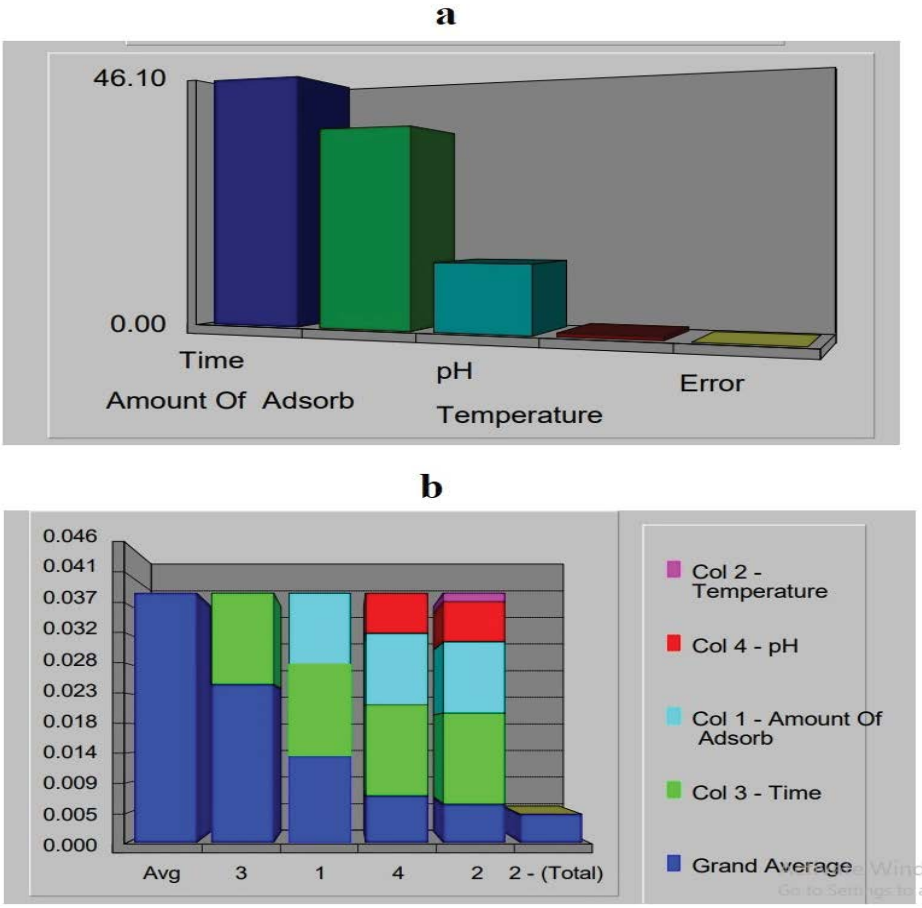

Fig. 8. (a) Optimum performance and (b) significant interaction for each factor.

Table 5
Calculated parameters of pseudo-first-order, pseudo-second-order, and intraparticle diffusion models

Model	Parameter	Value
Pseudo-first-order model	q_e (mg/g)	10.65
	K_1 (min^{-1})	0.03
	R^2	0.9668
Pseudo-second-order model	q_e (mg/g)	14.66
	K_2 (g/mg·min)	0.002
	R^2	0.9968
Intraparticle diffusion model	K_i (mg/g·$min^{1/2}$)	0.94
	C_i (mg/g)	2.45
	R^2	0.9848

Table 6
Thermodynamics parameters for the adsorption of humic acid

Adsorbent	Temperature (K)	$\Delta H°$ (J/mol)	$\Delta S°$ (J/mol·K)	$\Delta G°$ (J/mol)
3D/GO@AA-AGE/PG	298	–6,379.58	11.99	–9,954.04
	308			–10,073.9
	323			–10,253.8

3.5. Reusability of 3D/GO@AA-AGE/PG

The regeneration and reusability of the 3D/GO@AA-AGE/PG were studied (Fig. 9). For this test, the adsorption/desorption test was done under optimized conditions. 3D/GO@AA-AGE/PG after use was washed with 10 mL methanol. After that, ten consecutive cycles were done with the same method, and the data shown that the adsorption capacity of the 3D/GO@AA-AGE/PG had a negligible decrease in adsorption efficiency (100%–80%). The decrease in adsorption capacity after five cycles by 30% is related to bond breaking. Accordingly, this shows the high efficiency of the prepared 3D/GO@AA-AGE/PG for the removal of HA from aqueous solutions.

3.6. Analysis of real samples

Application of the developed technique was done by different water samples. The preparation of water samples were explained in the 2.7 section. The obtained data are listed in Table 7. Water samples were carried out by spiked HA. The obtained data were listed in Table 7 with the removal percentage for HA from the water sample ranged from

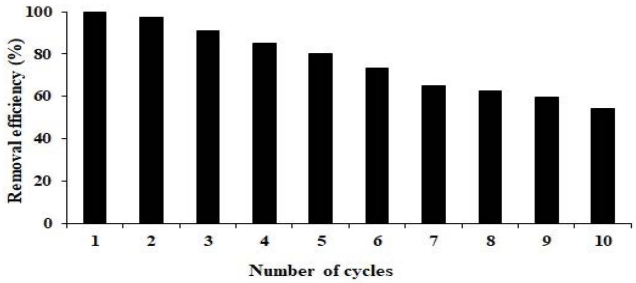

Fig. 9. Reusability of 3D/GO@AA-AGE/PG.

Table 7
Different removal percentages of humic acid in the water samples (n = 3)

Sample	Added (μg/mL)	Found (μg/mL)	RSD (%)	Removal (%)
Well water (Darakeh)	0.5	0.86	1.02	86.29
Well water (Manjilabad)	0.5	0.81	5.69	81.54

Table 8
Comparison of maximum adsorption capacity of several nanoadsorbents for removal of humic acid

Nanoadsorbent	Adsorption capacity	References
ZnO nanoparticle	0.81	[30]
Base-treated PAC	7.60	[31]
Natural maifan stone	1.00	[32]
Acid-activated Greek bentonite	10.75	[33]
3D/GO@AA-AGE/PG	13.31	Present study

81.59% to 86.29%, which shown that this procedure can be satisfactorily applied to the removal of HA in environmental water samples.

3.7. Comparison of adsorption capacity with other nanoadsorbents

Table 8 lists the comparison of adsorption capacity of various adsorbents for HA removal. The adsorption capacity of 3D/GO@AA-AGE/PG used in the present study is comparable with some other reported nanoadsorbents [30–33]. It can be concluded that GO/Fe_3O_4 and AA-AGE had a synergistic influence on HA removal in 3D/GO@AA-AGE/PG. These all exhibit that 3D/GO@AA-AGE/PG is a more appropriate and promising nanoadsorbent for treating water samples contaminated with HA.

4. Conclusion

In summary, a novel 3D/MNPs were prepared by surface modification of GO with AA and AGE as modifiers, and their sorption mechanisms for HA were studied. The FT-IR, FE-SEM/EDX, and TGA analyses were used to characterize the chemical composition and nanostructure of the nanoadsorbent from the proposed method. To minimize the number of experimental tests, energy and time, optimum solution pH, adsorbent dosage, temperature and contact time factors are obtained by the Taguchi method (L_9). ANOVA shown that the most significant parameter was contact time with 51.62% contribution. The removal efficiency of HA (%R > 58%) was obtained by using pH = 6, adsorbent dosage = 0.02 g, contact time = 120 min, and temperature = 25°C. The sorption mechanism could be well evaluated by the pseudo-second-order kinetic and Langmuir isotherm models. The thermodynamic data confirmed spontaneous, exothermic, and favorable HA sorption to 3D/GO@AA-AGE/PG. Also, the nanoadsorbent shows excellent reusability in the adsorption–desorption cycles.

Supporting information

Additional supporting information may be found in the Supporting Information section at the end of the article.

Acknowledgement

The authors would like to acknowledge Islamic Azad University (Science and Research Branch) for financial support of this work.

Funding

This research did not receive any specific grant from funding agencies in the public, commercial, or not-for-profit sectors.

Symbols

R%	—	Removal of humic acid
q_e	—	Adsorption capacity of humic acid
C_0	—	Initial concentrations of humic acid
C_t	—	t time concentrations of humic acid
C_e	—	Equilibrium concentrations of humic acid
V	—	Volume of solution
W	—	Weight of nanoadsorbent
q_{max}	—	Maximum sorption capacity of humic acid
K_L	—	Langmuir isotherm constant
K_F	—	Freundlich isotherm constant
β	—	Dubinin–Radushkevich isotherm constant
R	—	Universal gas constant
T	—	Temperature
b	—	Constant related to the heat of humic acid sorption
K_T	—	Temkin constant
ε	—	Polanyi potential
q_t	—	Sorption capacity at time
C_i	—	Intercept
K_1	—	Pseudo-first-order rate constant
K_2	—	Pseudo-second-order rate constant
K_i	—	Intraparticle diffusion rate constant
$\Delta H°$	—	Enthalpy change
$\Delta G°$	—	Free energy change
$\Delta S°$	—	Entropy change
K_L	—	Thermodynamic equilibrium constant

References

[1] S. Bousba, N. Bougdah, N. Messikh, P. Magri, Adsorption removal of humic acid from water using a modified Algerian, bentonite, Phys. Chem. Res., 6 (2018) 613–625.

[2] J. Wang, X. Han, H. Ma, Y. Ji, L. Bi, Adsorptive removal of humic acid from aqueous solution on polyaniline/attapulgite composite, Chem. Eng. J., 173 (2011) 171–177.

[3] H. Sehaqui, U.P. Larraya, P. Tingaut, T. Zimmermann, Humic acid adsorption onto cationic cellulose nanofibers for bioinspired removal of copper(II) and a positively charged dye, Soft Matter, 11 (2015) 5294–5300.

[4] E. Derakhshani, A. Naghizadeh, Optimization of humic acid removal by adsorption onto bentonite and montmorillonite nanoparticles, J. Mol. Liq., 259 (2018) 76–81.

[5] C.R.O. Melia, W.C. Becker, K.-K. Au, Removal of humic substances by coagulation, Water Sci. Technol., 40 (1999) 47–54.

[6] M.T. Ghaneian, M. Tabatabaee, P. Morovati, M.H. Ehrampoush, A. Dehghani, Photocatalytic degradation of humic acid by Ag/ZnO nanoparticles under UVC irradiation from aqueous solutions, J. Community Health. Res., 3 (2014) 153–161.

[7] M. Prisciandaro, A. Salladini, D. Barba, Membrane filtration of surface water for the removal of humic substances, 2008.

[8] G. Ji, S. Sun, R. Jia, J. Liu, Z. Yao, M. Wang, Q. Zhao, L. Hou, Study on the removal of humic acid by ultraviolet/persulfate advanced oxidation technology, Environ. Sci. Pollut. Res., 27 (2020) 26079–26090.

[9] Y. Zhou, L. Zhang, Z. Cheng, Removal of organic pollutants from aqueous solution using agricultural wastes: a review, J. Mol. Liq., 212 (2015) 739–762.

[10] I. Ali A. Mohd, T.A. Khan, Low cost adsorbents for the removal of organic pollutants from wastewater, J. Environ. Manage., 113 (2012) 170–183.

[11] Y. Park, G.A.A. Yoko, R. Kurdi, E. Horváth, J. Kristóf, R.L. Frost, Adsorption of phenolic compounds by organoclays: implications for the removal of organic pollutants from aqueous media, J. Colloid Interface Sci., 406 (2013) 196–208.

[12] S.H. Al-Rekabi, Y. Mustapha Kamil, M.H. Abu Bakar, Y.W. Fen, H.N. Lim, S. Kanagesan, M.A. Mahdi, Hydrous ferric oxide-magnetite-reduced graphene oxide nanocomposite for optical detection of arsenic using surface plasmon resonance, Opt. Laser Technol., 111 (2019) 417–423.

[13] A. Maleki, R. Rahimi, S. Maleki, Efficient oxidation and epoxidation using a chromium(VI)-based magnetic nanocomposite, Environ. Chem. Lett., 14 (2016) 195–199.

[14] J. Wang, L. Bi, Y. Ji, H. Ma, X. Yin, Removal of humic acid from aqueous solution by magnetically separable polyaniline: adsorption behavior and mechanism, J. Colloid Interface Sci., 430 (2014) 140–146.

[15] Y. Yao, S. Miao, S. Yu, L. Ping Ma, H. Sun, S. Wang, Fabrication of Fe_3O_4/SiO_2 core/shell nanoparticles attached to graphene oxide and its use as an adsorbent, J. Colloid Interface Sci., 379 (2012) 20–26.

[16] Y. Ren, H.A. Abbood, F. He, H. Peng, K. Huang, Magnetic EDTA-modified chitosan/SiO_2/Fe_3O_4 adsorbent: preparation, characterization, and application in heavy metal adsorption, Chem. Eng. J., 226 (2013) 300–311.

[17] J. Wang, S. Zheng, Y. Shao, J. LiangLiu, Z. Xu, D. Zhu, Amino-functionalized Fe_3O_4@SiO_2 core–shell magnetic nanomaterial as a novel adsorbent for aqueous heavy metals removal, J. Colloid Interface Sci., 349 (2010) 293–299.

[18] S. Zhang, Y. Zhang, J. Liu, Q. Xu, H. Xiao, X. Wang, H. Xu, J. Zhou, Thiol modified Fe_3O_4@SiO_2 as a robust, high effective, and recycling magnetic sorbent for mercury removal, Chem. Eng. J., 226 (2013) 30–38.

[19] Y. Yang, X. Hu, Y. Zhao, L. Cui, Z. Huang, J. Long, J. Xu, J. Deng, C. Wu, W. Liao, Decontamination of tetracycline by thiourea-dioxide–reduced magnetic graphene oxide: Effects of pH, ionic strength, and humic acid concentration, J. Colloid Interface Sci., 495 (2017) 68–77.

[20] Y. Wang, S. Liang, B. Chen, F. Guo, S. Yu, Y. Tang, Synergistic removal of Pb(II), Cd(II) and humic acid by Fe_3O_4@mesoporous silica-graphene oxide composites, PLoS One, 11 (2013) 65634, doi: 10.1371/journal.pone.0065634.

[21] M. Wang, L. Cai, Q. Jin, One-pot composite synthesis of three-dimensional graphene oxide/poly(vinyl alcohol)/TiO_2 microspheres for organic dye removal, Sep. Purif. Technol., 172 (2017) 217–226.

[22] H. Vojoudi, A. Badiei, A. Banaei, S. Bahar, S. Karimi, G.M. Ziarani, M.R. Ganjali, Extraction of gold, palladium and silver ions using organically modified silica-coated magnetic nanoparticles and silica gel as a sorbent, Microchim. Acta, 184 (2017) 3859–3866.

[23] I. Langmuir, The adsorption of gases on plane surfaces of glass, mica and platinum, J. Am. Chem. Soc., 40 (1918) 1361–1403.

[24] H.M.F. Freundlich, Über die Adsorption in Lösungen, Z. Phys. Chem., 57 (1906) 385–470.

[25] M.I. Temkin, Adsorption equilibrium and kinetics of processes on heterogeneous surfaces and at interaction between adsorbed molecules, Zh Fiz Khim (Russ. J. Phys. Chem.), 15 (1941) 296–332.

[26] M.M. Dubinin, The potential theory of adsorption of gases and vapors for adsorbents with energetically non-uniform surface, Chem. Rev., 60 (1960) 235–266.

[27] A.B. Albadarin, M. Charara, B.M.A. Tarboush, M.N.M. Ahmad, T.A. Kurniawan, N. Mu, mechanism Analysis of tartrazine biosorption onto masau stone, a low cost by-product from semi-arid regions, J. Mol. Liq., 242 (2017) 478–483.

[28] S. Suganya, P.S. Kumar, Kinetic and thermodynamic analysis for the redemption of effluents containing Solochrome Black T onto powdered activated carbon: a validation of new solid-liquid phase equilibrium model, J. Mol. Liq., 259 (2018) 88–101.

[29] Z. Berizi, S.Y. Hashemi, M. Hadi, A. Azari, A.H. Mahvi, The study of non-linear kinetics and adsorption isotherm models for acid red 18 from aqueous solutions by magnetite nanoparticles and magnetite nanoparticles modified by sodium alginate, Water Sci. Technol., 74 (2016) 1235–1242.

[30] V. Oskoei, M.H. Dehghani, S. Nazmara, B. Heibati, M. Asif, I. Tyagi, S. Agarwal, V.K. Gupta, Removal of humic acid from aqueous solution using UV/ZnO nano-photocatalysis and adsorption, J. Mol. Liq., 213 (2016) 374–380.

[31] K. Yang, J.T. Fox, Adsorption of humic acid by acid-modified granular activated carbon and powder activated carbon, J. Environ. Eng., 144 (2018) 04018104, doi: 10.1061/(ASCE) EE.1943-7870.0001390.

[32] H. Yang, B. Luo, Y. Zhang, B. Zhou, S. Manzoor Ahmed, H. Liu, X. Liu, Y. He, S. Xia, Study of humic acid adsorption character on natural maifan stone: characterization, kinetics, adsorption isotherm, and thermodynamics, ACS Omega, 5 (2020) 7683–7692.

[33] D. Doulia, C. Leodopoulos, K. Gimouhopoulos, F. Rigas, Adsorption of humic acid on acid-activated Greek bentonite, J. Colloid Interface Sci., 340 (2009) 131–141.

Supporting information

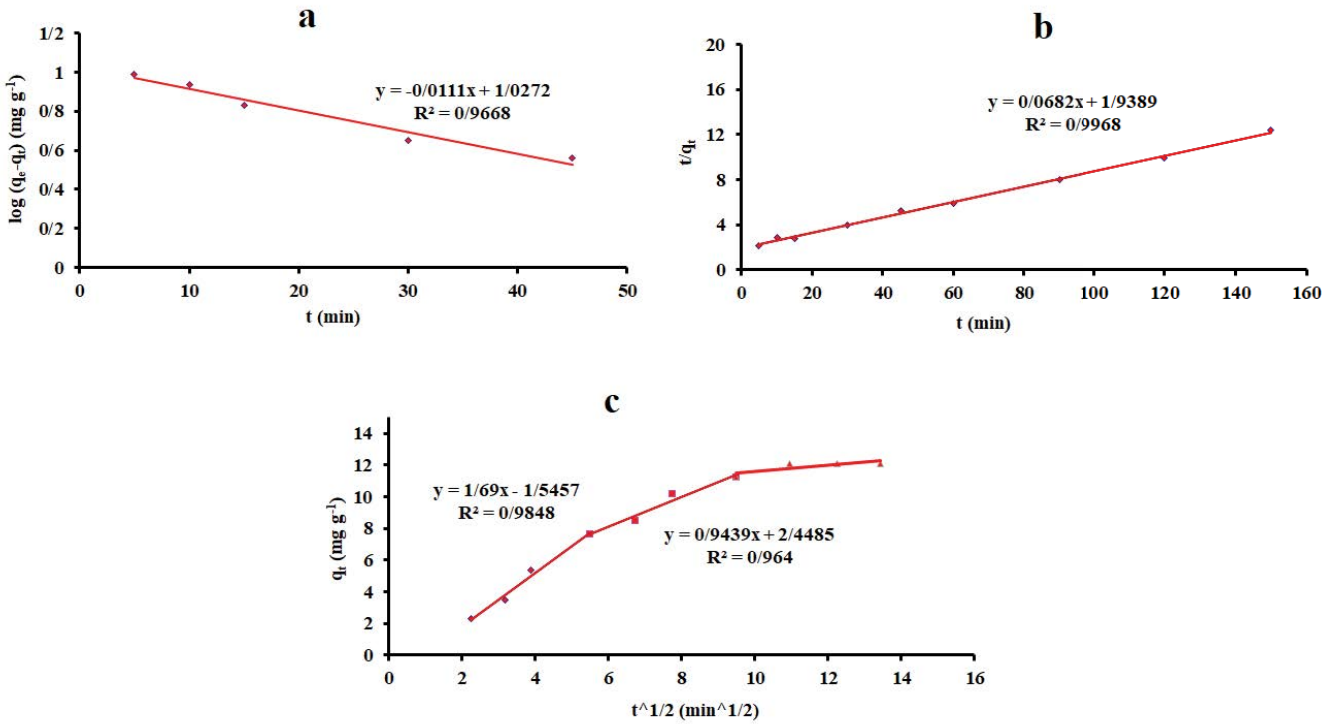

Fig. S1. Kinetics curve for the sorption of humic acid on 3D/GO@AA-AGE/PG: (a) pseudo-first-order model, (b) pseudo-second-order model, and (c) intraparticle diffusion model (adsorbent dosage, 0.015 g; temperature, 25°C; initial concentration: 20 mg/L; pH 6).

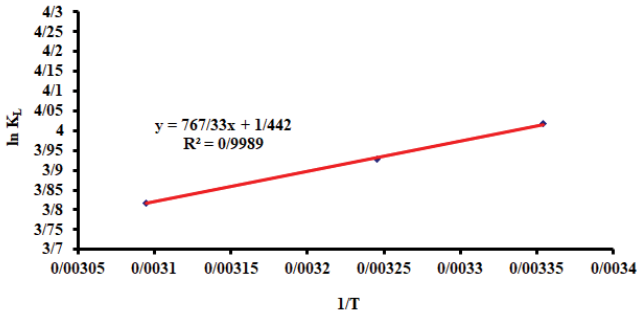

Fig. S2. Plot of lnK_L and 1/T.